Carbohydrate Polymers 92 (2013) 1100–1106

Contents lists available at SciVerse ScienceDirect

Carbohydrate Polymers

journal homepage: www.elsevier.com/locate/carbpol

# Diameter-tuning of electrospun cellulose acetate fibers: A Box–Behnken design (BBD) study

Rocktotpal Konwarh[a,1], Manjusri Misra[a], Amar K. Mohanty[a], Niranjan Karak[b,*]

[a] Department of Plant Agriculture, University of Guelph, Ontario N1G2W1, Canada
[b] Department of Chemical Sciences, Tezpur University, Napaam, Sonitpur, Assam 784028, India

ARTICLE INFO

*Article history:*
Received 4 April 2012
Accepted 22 October 2012
Available online 30 October 2012

*Keywords:*
Cellulose acetate nanofiber
Process optimization
Electrospinning
Response surface methodology
Scanning electron microscope

ABSTRACT

This work focuses on the use of statistical approach in optimizing shape-size accord of electrospun cellulose acetate (CA) mats – an apt material for biomedical and industrial applications. Modulation of three processing parameters, namely potential difference, distance between tip-to-collector and feed rate led to myriad of fiber-morphology (beaded, bead free, branched and ribbon) with diverse size-spectrum. Response surface methodology using Box–Behnken design technique indicated significant linear and quadratic influence of the chosen parameters. Fibers with minimal diameter of ~139 nm (with a mean coherency co-efficient of 0.5192) were predicted for 30 kV (voltage), 15 cm (tip-to-collector distance) and 2 mL/h (feed rate). Reasonable agreement existed between the predicted *R*-squared value (0.9565) and adjusted *R*-squared value (0.9824) with similar observation for the experimental and model values over the entire factor space. The developed model may serve as a base model for understanding process – parametric influence on electrospinning CA and related polymers.



## 1. Introduction

The technique of electrospinning has ushered in various novel applications of polymeric fibers (ranging from 3 nm to greater than 5 μm in diameter) across different domains (Subbiah, Bhat, Tock, Parameswaran, & Ramkumar, 2005). The basic framework of electrospinning is shown in Fig. 1. Electrospinning, being a multi-parameter-dictated process, demands an inevitable optimization of the solution-property, ambient variables and the processing conditions to fine tune the shape-size unison of the electrospun fibers (Doshi & Reneker, 1995) that eventually dictates their bio-physico-chemico attributes.

In the wide milieu of application-oriented electrospun fibers, cellulose acetate (CA) nanofibers have carved a unique niche of their own as biomimetic tissue engineering scaffolds (Rubenstein et al., 2010), biomolecule-immobilization platforms (Chen, Huang, et al., 2011; Chen, Wang, & Huang, 2011; Phachamud & Phiriyawirut, 2011), bioremediation mats (Xiao et al., 2009), and energy storage materials (Chen, Huang, et al., 2011; Chen, Wang, et al., 2011), amongst others. A handful of work (Haas, Heinrich, & Greil, 2010; Han, Youk, Min, Kang, & Park, 2008) has focussed upon suitability of different solvent systems for electrospinning cellulose acetate. In the context of issues related to toxicity of various conventionally used organic solvents (Haas et al., 2010), the recent reports on the use of binary mixture of water (considered as a green solvent) and acetic acid for electrospinning CA is attractive (Han et al., 2008). Vrieze et al. (2009) have studied the effect of ambient parameters including relative humidity and temperature on the diameter of the electrospun CA nanofibers. However, reports on the effect of the electrospinning process parameters like applied potential, feed rate and so on are not available. Though the influence of these parameters on the fiber diameter has often been investigated individually, elucidation of the cross-effect or interaction effects among the chosen parameters is expected to present a more convincing picture. A narrow-size window of electrospun fibers may be indispensable for a number of applications, as for example, to mimic the extracellular matrix in a better way during tissue engineering applications or to increase the drug-loading percentage, dependent on the surface area to volume ratio of the fibers.

A number of studies have focussed on optimizing the processing parameters for various electrospun materials like silk (Amiraliyan, Nouri, & Kish, 2009), poly(D,L-lactide) (Gu & Ren, 2005) and titanium dioxide (Ray & Lalman, 2011) using different statistical approaches. In this context, response surface methodology (RSM) is often viewed as a suitable aid to designing experiments. It is an apt choice in developing numerical models, measuring the

* Corresponding author. Tel.: +91 3712 267009; fax: +91 3712 267006.
*E-mail address:* karakniranjan@yahoo.com (N. Karak).
[1] Present address: Department of Chemical Sciences, Tezpur University, Napaam, Sonitpur, Assam 784028, India.

0144-8617/$ – see front matter © 2012 Elsevier Ltd. All rights reserved.
http://dx.doi.org/10.1016/j.carbpol.2012.10.055

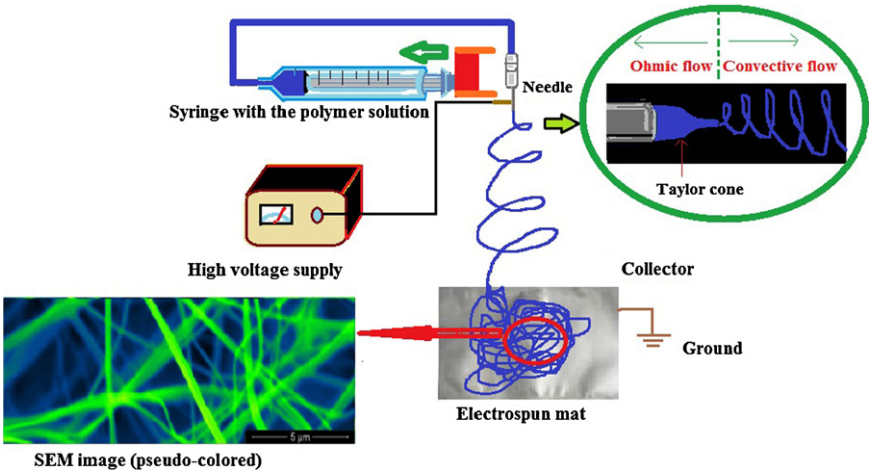


**Fig. 1.** Electrospinning – the basic framework.

influence of variables and the hunt for optimum combinations of variables (Meyer & Montogomery, 2002). In a recent review, Bezerra, Santelli, Oliveira, Villar, and Escaleira (2008) have focussed on the suitability of RSM in optimization studies. The prime steps of RSM are: (1) to choose the independent variables of major effects on the system post screening studies, delimit the experimental region in accordance to the study-objective and the researcher's experience; (2) to select an experimental design and execute the experiments in the context of the selected experimental matrix; (3) to fit a polynomial function of the experimental data via the latter's mathematic–statistical treatment; (4) to assess the model's fitness; (5) to verify the inevitability and option of executing a displacement in direction to the ideal/optimal region; and (6) to obtain the optimum values of the variables under consideration. Codification of the levels of the variable is important in RSM. Each studied real value is transformed into coordinates within a scale with dimensionless values. This should be proportional at its localization in the investigational domain. Codification facilitates the analysis of variables of varied orders of magnitude without the greater affecting the assessment of the lesser. The following equation can be applied to transform a real value ($z_i$) into a coded value ($x_i$) according to a determinate experimental design:

$$x_i = \left( \frac{z_i - z_i^o}{\Delta z_i} \right) \beta_d \quad (1)$$

where, $z_i$ is the distance between the real value in the central point and the real value in the higher or lower level of a variable, $\beta_d$ is the major coded limit value in the matrix for each variable, and $z_i^o$ is the real value in the central point.

This paper highlights the use of Box–Behnken design (BBD) as an optimization tool to minimize the diameter of electrospun CA fibers. It is pertinent to mention that the use of BBD is often advantageous when compared to central composite design (CCD) for a quadratic response surface model with three or more factors (Ray & Lalman, 2011). Using the system reported by Han et al. (2008) as reference for our study, we wanted to evaluate the effect of modulating the process parameters like applied potential, tip-to-collector distance and feed rate on the diameter of electrospun CA fibers. The objective was to assess whether such parametric modulations subjected to statistical optimization can be really useful to reduce the average diameter of the CA nanofibers or not.

## 2. Experimental

### 2.1. Materials

Cellulose acetate, CA (acetyl content 39.8%, average $M_n$ = 30,000 by GPC) and acetic acid (~99.5% pure) were purchased from Aldrich and ACROS respectively. Milli-Q water was used throughout the experiment.

### 2.2. Electrospinning and characterization

Cellulose acetate dissolved in acetic acid and Millipore water (75:25, w/w) (abbreviated to AcW) was electrospun in ME MECC NANON 01 electrospinning machine (Canada Foundation for Innovation) under different parametric modulations of voltage, tip-to-collector distance and feed rate as outlined in subsequent sections (relative humidity, $R_H$ = 29–32% and temperature = 23 °C). The viscosity of the AcW solution was found to be ~5500 cP as determined using Brookefield digital viscometer at room temperature (~23 °C).

Scanning electron microscope (SEM, INSPECT$^{TM}$ S50-FEI) was used to observe the morphology of the electrospun CA fibers post gold coating for about 40 s in Cressington Sputter coater. Image analysis processing as developed by Shin, Cho, Seo, and Kim (2008) was used to determine the distribution of the electrospun fiber diameter. In brief, the analysis consisted of two phases. The first phase comprised of generation of threshold and binary images of the acquired SEM image, followed by boundary detection. It is pertinent to mention that Canny Edge detecting method was applied to separate the boundary of each fiber at the fiber-to-fiber crossover areas. In the second phase, skeletonization was used to define the fiber center line. The distance from the center to the boundary was calculated using distance transform. While a manual method for calculating the size of the beads was used in case of the beaded fibers. Fiji was used for evaluating orientation and coherency of the fibers electrospun under optimized process parameters.

### 2.3. Experimental design, model development and verification

In order to assess the effect of varying electrospinning parameters on the generation of CA fibers, BBD technique was used to estimate the main effects on the response i.e., the diameter of the electrospun nanofibers ($Y$). Applied voltage ($A$), distance between the tip and the collector ($B$) and feed rate ($C$) were the selected

**Table 1**
Box–Behnken design matrix containing 17 experimental runs.

| Run order | Applied potential (kV) | Tip-to-collector distance (cm) | Feed rate (mL/h) | Response, *Y* (fiber diameter in nm) |
|---|---|---|---|---|
| 6 | 30 | 13 | 1 | 144 |
| 10 | 25 | 15 | 1 | 141 |
| 9 | 25 | 11 | 1 | 151 |
| 16 | 25 | 13 | 2 | 144 |
| 12 | 25 | 15 | 3 | 145 |
| 5 | 20 | 13 | 1 | 153 |
| 14 | 25 | 13 | 2 | 143.8 |
| 11 | 25 | 11 | 3 | 153 |
| 8 | 30 | 13 | 3 | 147 |
| 2 | 30 | 11 | 2 | 148 |
| 4 | 30 | 15 | 2 | 139 |
| 13 | 25 | 13 | 2 | 143.8 |
| 7 | 20 | 13 | 3 | 156 |
| 3 | 20 | 15 | 2 | 151 |
| 15 | 25 | 13 | 2 | 144.2 |
| 17 | 25 | 13 | 2 | 144 |
| 1 | 20 | 11 | 2 | 160 |

independent variables. The three factors with three levels consisting of 17 experimental runs were used to analyse the experimental data including multiple replicates at the centre point (Haaland, 1989). This conveys additional information in the interior of the investigational region complemented by better appraisal of the experimental error. Coded values ((−1 for $A = 20$ kV, $B = 11$ cm and $C = 1$ mL/h; 0 for $A = 25$ kV, $B = 13$ cm and $C = 2$ mL/h; 1 for $A = 30$ kV, $B = 15$ cm and $C = 3$ mL/h) were used for the analysis. Table 1 represents the design matrix for experimental factors and response. Based on this design, the second order polynomial Eq. (2), comprising of individual and cross effect of each variable was used to fit the experimental data.

$$Y = a_0 + a_1A + a_2A^2 + a_3B + a_4B^2 + a_5C + a_6C^2 + a_7A \times B + a^8A \times C + a_9B \times C \quad (2)$$

where $a_0$, $a_1$, $a_2$, $a_3$, $a_4$, $a_5$, $a_6$, $a_7$, $a_8$, $a_9$ are the regression coefficients. Analyses were carried out in triplicates. The data tabulated were (Table 1) the average of two sets of measurements. An analysis of variance (ANOVA) of the experimental response was performed to assess the full quadratic approximation of the BBD response surface model. The statistical computations were performed using the software Design-Expert 8.0.6. The significance of each coefficient was determined from the *t*-values and *p*-values. Co-efficients in the equation with *t*-values greater than *t*-values at 95% level of confidence or $p > 0.05$ were considered statistically significant. The final response surface model was further refined by deleting the terms found to be associated with a level of significance greater than 5% ($p > 0.05$) (Box & Draper, 1987).

## 3. Results and discussion

RSM is employed to appraise the relations existing among a group of controlled investigational factors and the observed response of one or more chosen criteria. A preliminary knowledge of the studied process aids in achieving a realistic model. In the present context, the utility of RSM was assessed for elucidating the influence of few selected process parameters on the diameter of electrospun CA fibers. It is needless to mention about the intricate play of different process parameters in electrospinning. Application of a high potential difference leads to charge induction and gradual build-up of repulsive force (thereby imposing an electrical polarization stress) with subsequent elongation of the polymer fluid drop, held at a needle tip by surface tension. The charge repulsion at some threshold potential difference overcomes the surface tension along with the viscous forces within the fluid drop. A complex force-balance dictates the ejection of fluid jet and subsequent formation of nanofibers. Shin, Hohman, Brener, and Rutledge (2001) have demonstrated the instability and whipping movement with high frequency of the ejected jet post traveling a short distance (using high speed photography with exposure times as low as 18 ns). They have modeled the behavior of the jet in terms of three instabilities:

(a) Axisymmetric Rayleigh instability, dominated by surface tension. This is suppressed at high electric fields or charge densities.
(b) Conducting mode instabilities, independent of the surface tension: (i) axisymmetric and (ii) non-axisymmetric (whipping instability).

The dominant mode varies in response to various applied fields and feed rate, which eventually dictate the fiber diameter.

### 3.1. Backdrop of the selected levels of the chosen parameters

We present the response surface model developed for the electrospun CA nanofibers in the subsequent sections. However, the readers would be intrigued about the backdrop of setting the aforestated levels of the selected factors. This selection was based on the available resources and results from preliminary experiments (feasibility study). In the process-parameters optimization for electrospun titanium dioxide, Ray and Lalman (2011) have pointed out the production of electrical arcs between the electrodes (as the static potential exceeds the resistance of the enclosed air inside the chamber) to be responsible for discontinuous withdrawal of fluid jet beyond the selected highest potential difference and lowest separation distance. In our study, three levels of the potential difference were distributed between 20 kV and 30 kV. It was difficult to observe a continuous fiber formation without sputtering of the polymer solution below the lowest selected potential difference (<20 kV). This may be attributed to the lower net effect of the applied voltage than the opposing forces on the solution droplet at the needle tip. A potential difference of 30 kV (the maximal limit of the electrospun machine used) across the separation distance of 15 cm could draw an uninterrupted strand of fluid jet with continuous fiber formation. At feed rates greater than 3 mL/h, particularly at higher values of the applied potential difference voltage resulted in beaded fibers (Fig. 2a). At very high feed rates (>3 mL/h), electrospinning of the fibers was intermittent. The sporadic behavior may be attributed to the short residence time of the drop and solidification of an accumulated mass of the polymer

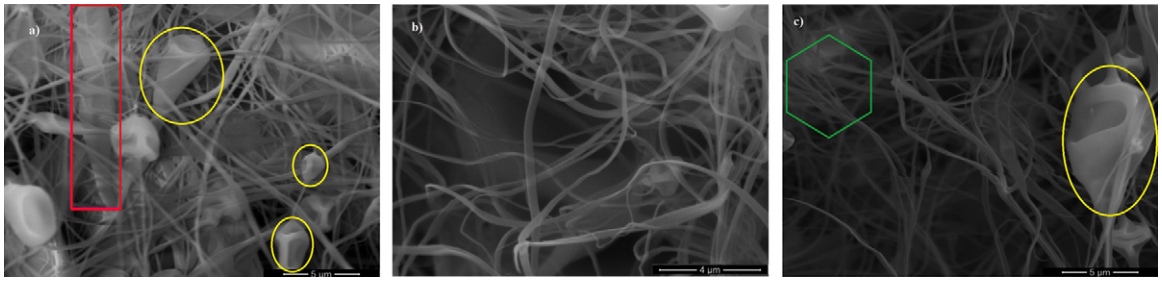


**Fig. 2.** SEM micrographs of few feasibility experiments (details in the text) – the yellow (circular), red (rectangular) and green (hexagonal) boundaries are meant to indicate the beads, flattened structure (probably due to solvent-impact) and branched structures respectively. (For interpretation of the references to color in this figure legend, the reader is referred to the web version of the article.)

solution at the needle tip. The fibers electrospun under high potential difference (30 kV), short separation distance between tip and collector (11 cm) and high feed rate (3 mL/h) were bead-free and appeared flat and ribbon-like though the maximal number of fibers in the observed microscopic fields had considerably large diameter (Fig. 2b). It is pertinent to mention that Han et al. (2008) have reported the controlling of the average diameters of the CA nanofibers from 160 nm to 1280 nm as a function of the composition of the mixed solvent of acetic acid and water. Considering the minimal separation distance of 10 cm as reported by them for rotatory collector, we initially intended to select this as the central value for our plate collector system as well. Interestingly, electrospinning with a separation distance below this value (<10 cm) at potential difference set at 30 kV, highly polydispersed fibers (size spectrum: 153–1185 nm) with mixed morphology including branched architecture (like dendritic branching) (Fig. 2c) could be observed. Spindle-shaped beads as large as about 9 μm were also noted. Henceforth, the selected levels for the tip-to-collector level ranged from 11 cm to 15 cm. These observations were indicative of the existence of certain optimal process parametric values. Under these optimal settings, the residence time for drop formation at the needle tip along with increased 'time-of-flight' for the charged ejected jet are supposed to augment the solvent evaporation and consequently enhance the sol–gel conversion into solid phase.

### 3.2. Response surface model

As noted previously, the cellulose acetate fibers were electrospun at each design point of the three chosen variables (potential difference, tip-to-collector distance and feed rate) and three levels of the BBD. The diameter of the fibers (i.e., the response) generated from each experiment was measured and the average of two sets of experiments was documented in the column *Y* in Table 1.

Initially, sequential model sum of squares (Type I) was used to select the highest order polynomial where the additional terms are significant and the model is not aliased. The sequential *p*-value <0.0001 suggested a quadratic model although the model summary statistics was suggestive to focus on the model, maximizing adjusted *R*-squared (0.97393) and the predicted *R*-squared (0.8584). In order to evaluate the quadratic response surface model, the experimental data was then subjected to an analysis of variance (ANOVA) using partial or Type III sum of squares (SS) that calculates the SS for a term post correction for all other terms in the model. The ANOVA results (Table 2) showed that the model was statistically significant with linear and quadratic terms. Values of "Prob > *F*" less than 0.0500 indicated the significant model terms. In this case $A$, $B$, $C$, $A^2$, $B^2$, $C^2$ were found to be significant model terms. Model reduction is a common strategy to improve the model in case there are many insignificant model terms (not including those required to support hierarchy). In order to get a refined response surface model, the statistically insignificant terms ($p > 0.05$) were deleted from the full quadratic model according to the backward elimination method (Ray & Lalman, 2011). It was interesting to note that only the linear and quadratic terms for the three electrospinning variables found place in the refined model. The model *F*-value of 149.72 implied the model to be statistically significant. There was only a 0.01% chance that a "model *F*-value" this large could occur due to noise.

The pred *R*-squared of 0.9565 was in reasonable agreement with the adj *R*-squared of 0.9824 in the refined model. The experimental fiber diameter versus the model predicted diameter is shown in Fig. 3. Computation of the linear correlation coefficient suggested a reasonable agreement between the experimental and model values over the entire factor space under consideration. The 'adequate precision' measures the signal to noise ratio. A ratio greater than 4 is desirable. In this case, a value of 40.565 indicated an adequate signal and therefore the model could be used to navigate the design space. The refined response surface model comprising of terms which are statistically significant at $p < 0.05$ is represented in the following equation:

$$\text{CA fiber diameter} = 143.96 - 5.25 \times A - 4.5 \times B + 1.5 \times C + 4.02 \times (A)^2 + 1.52 \times (B)^2 + 2.02 \times (C)^2 \quad (3)$$

### 3.3. Perturbation plot

A Perturbation plot is like "one factor at a time" investigation. However, these plots aid in a comparative assessment of the influence of all the factors at a particular point in the design space. Only one factor is modulated over its range while all the other factors are held constant. By default, the reference point is set at the midpoint (coded 0) of all the factors in Design-Expert. We modulated the value of each variable between +1 and −1 levels, keeping the other two corresponding variables constant to assess the respective effect on the fiber diameter. A steep slope or curvature in a factor shows that the response is sensitive to that factor. A relatively

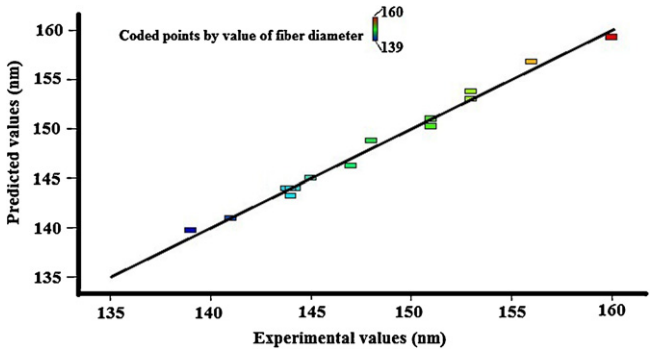


**Fig. 3.** Plot of model-predicted versus observed response (fiber diameter).

**Table 2**
ANOVA for response surface reduced quadratic model.

| Source | Sum of squares (SS) | Degrees of freedom (DF) | *F*-Value | *p*-Value prob > *F* |
|---|---|---|---|---|
| Model (significant) | 504.15 | 6 | 149.72 | <0.0001 |
| *A* | 220.50 | 1 | 392.91 | <0.0001 |
| *B* | 162.00 | 1 | 288.67 | <0.0001 |
| *C* | 18.00 | 1 | 32.07 | 0.0002 |
| $A^2$ | 68.04 | 1 | 121.25 | <0.0001 |
| $B^2$ | 9.73 | 1 | 17.33 | 0.0019 |
| $C^2$ | 17.18 | 1 | 30.61 | 0.0002 |

flat line shows insensitivity to change in that particular factor. The plots (Fig. 4) revealed that the fiber diameter is sensitive to change in each of the three chosen variables – the applied potential difference, tip-to-collector separation distance and feed rate. We have shown, for reference, the influence of change in voltage (Fig. 4a, i–v), separation distance (Fig. 4b, vi–x) and feed rate (Fig. 4c, xi–xv) by keeping the other two corresponding parameters at their central values. Fibers electrospun under a separation distance of 13 cm and feed rate of 2 mL/h showed a progressive decrease in fiber diameter with increase in applied potential. Greater the separation distance, smaller is the fiber diameter (at potential difference of 25 kV and 2 mL/h feed rate). Under a potential difference of 25 kV and 13 cm separation distance, a feed rate of 2 mL/h was found to be optimal for minimal fiber diameter. We have tried to present the plausible explanation of the observed trends with a greater insight into the influence of the chosen variables on the fiber diameter through the response surface plots in the subsequent section.

### 3.4. Response surface plots

The three dimensional surface plots of the response variable, CA fiber diameter (nm) versus two-variables-at-a-time (keeping the third variable constant at the central value, 0) are depicted in Fig. 5. A number of interesting observations emanate from these plots. Considering, Fig. 5a, fibers were minimal diameter were produced for the combination of highest potential difference (30 kV) with the maximal separation between the tip and the collector (15 cm) (the feed rate considered is 2 mL/h). On the other hand, decreasing the voltage to the minimum (20 kV) and feeding the polymer solution at the maximum rate of 3 mL/h led to the generation of fibers with the highest diameter (∼160 nm) (tip-to-collector distance = 13 cm) (Fig. 5b). Altering the central value, 0 of the third variable to +1 and −1 levels in the software (images not shown) yielded other interesting plots. A few generalized inferences were drawn from such plots regarding the electrospun cellulose acetate fibers: (a) the fiber diameter bore an inverse relationship to the potential difference over all the levels under consideration, (b) regardless of the applied voltage, increasing the distance of separation led to decrease in fiber diameter, and (c) the fiber diameter was minimal for the central value of feed rate i.e., 2 mL/h under all levels of applied potential difference. The SEM micrograph of the electrospun fibers generated under the optimal conditions is shown in Fig. 6. The average diameter of the fibers was calculated to be around 139 nm. A mean coherency co-efficient of 0.5192 was calculated using the software Fiji. A coherency co-efficient close to 1, represented as a slender ellipse, indicates a strongly coherent orientation of the local fibers in the direction of the ellipse long axis. A coherency co-efficient close to zero, represented as a circle, denotes no preferential orientation of the fibers.

Ramakrishna, Fujihara, Teo, Lim, and Ma (2005, chap. 3) have presented the effects of various electrospinning parameters on fiber-diameter and their shape-size accord of different polymeric materials. Our experimental observations of differential fiber diameter of electrospun cellulose acetate in response to parametric modulations are vouched by a number of comprehensive reports on electrospinning as discussed underneath.

Solution property to a large extent dictates the effect of varying the distance between the tip and the collector (profoundly affecting the flight-time and the field strength) on the fiber morphology. Interestingly, a couple of contrary reports exist as far as the separation distance and fiber diameter is concerned. Often the formation of beads has been reported for too short separation between the

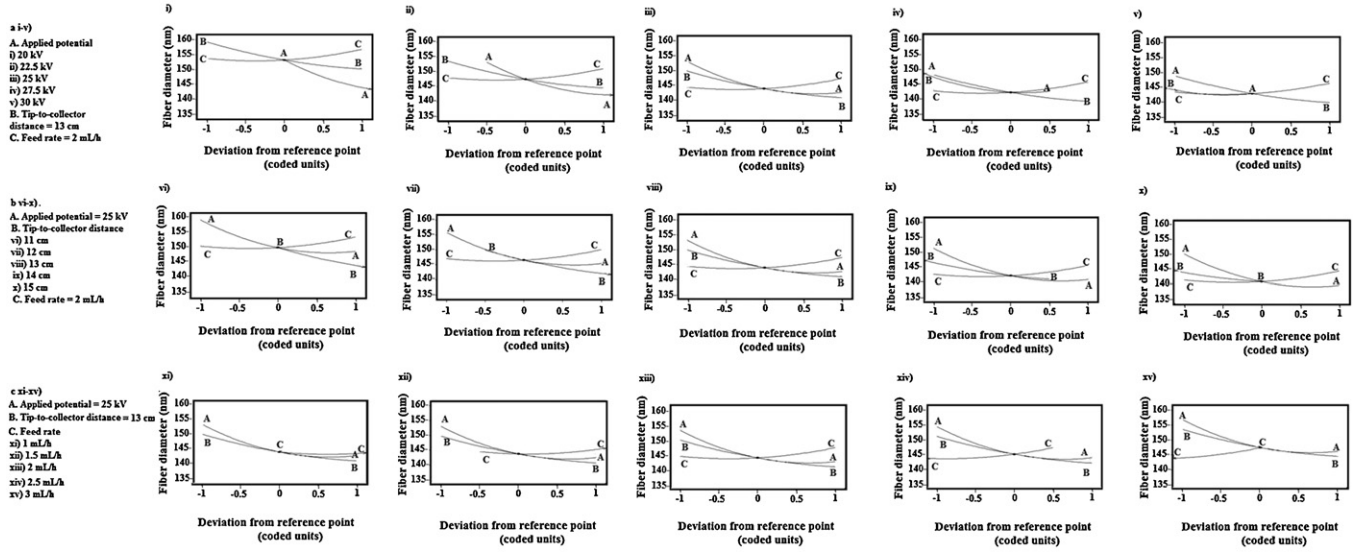


**Fig. 4.** Perturbation plots showing the effect of modulation in (a, i–v) applied potential, (b, vi–x) tip-to-collector distance and (c, xi–xv) feed rate (with the other two corresponding parameters remaining constant in each case) on the fiber diameter.

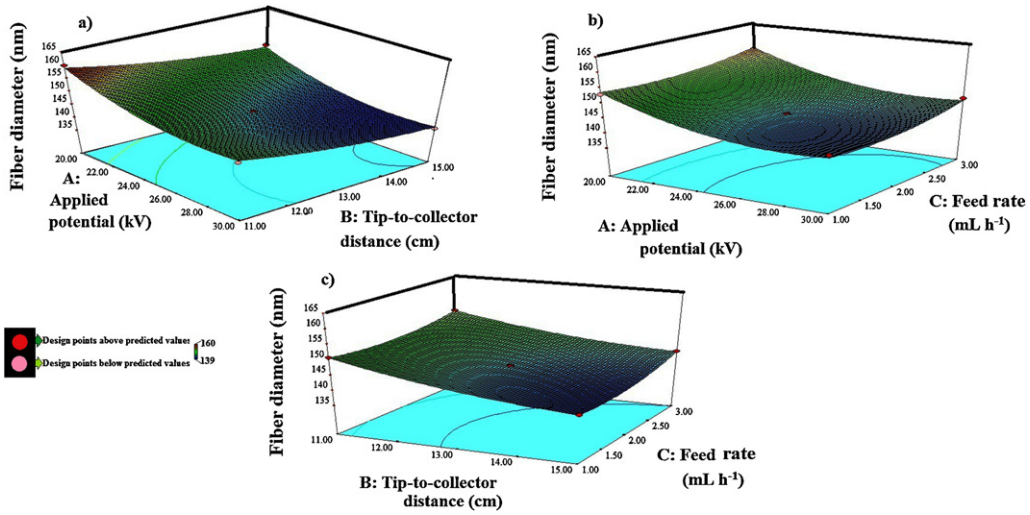


**Fig. 5.** Response surface plots of fiber diameter versus (a) applied potential versus separation distance, (b) applied potential versus feed rate and (c) separation distance versus feed rate.

tip and the collector due to increased field strength (Megelski, Stephens, Chase, & Rabolt, 2002) resulting in the increased instability of the jet. An increased separation has been associated with decreased fiber diameter in terms of longer flight time for the solution to be stretched prior to deposition on the collector (Zhao, Wu, Wang, & Huang, 2004). On the contrary, Lee et al. (2004) reported the increase in fiber diameter corresponding to increase separation distance in terms of decrease in field strength. However, Zhao et al. (2004) reported that fibers are not deposited if the separation distance is too high. Thus it appears that the stretching and acceleration of the jet (consequently the morphology and diameter of the electrospun fibers) are profoundly affected by the supplied voltage and the resultant electric field. Various studies have shown that higher voltage leads to greater stretching of the solution owing to greater columbic forces in the jet, consequently reducing the fiber-diameter (Lee et al., 2004; Megelski et al., 2002). It is important to note that the viscosity of 17 wt% cellulose acetate solution was only about 5500 cP. It was interesting to note that at higher voltage, secondary jets were also generated. A higher voltage is envisaged to favour the formation of secondary jets when a polymeric solution of lower viscosity is electrospun. This results in reducing the fiber diameter (Demir, Yilgor, Yilgor, & Erman, 2002). However, the formation of beads cannot be completely overlooked on application of very high voltage, which is often co-related with decreased flight-time of the polymer solution (due to greater stretching) and its recession into the needle-tip. The consideration of feed rate is very important at this juncture. In an interesting observation, Krishnappa, Desai, and Sung (2003) reported that increasing voltage will increase the beads density, which at an even higher voltage, the beads will join to form a thicker diameter fiber. This may also partially explain the observation of Fig. 2a.

Thus, it is confirmed that the different electrospinning parameters work to varied extents in influencing the fiber diameter. However, the authors would like to mention the important limitation of the study in terms of limited number of variables chosen. This work may be extended to understand the concomitant roles of the environmental factors and the solution properties. It also leaves the scope for delving into the effect of plausible modulations in the electrospinning process parameters on the fiber diameter in presence of polymers like poly(ethylene glycol), often blended with CA fibers.

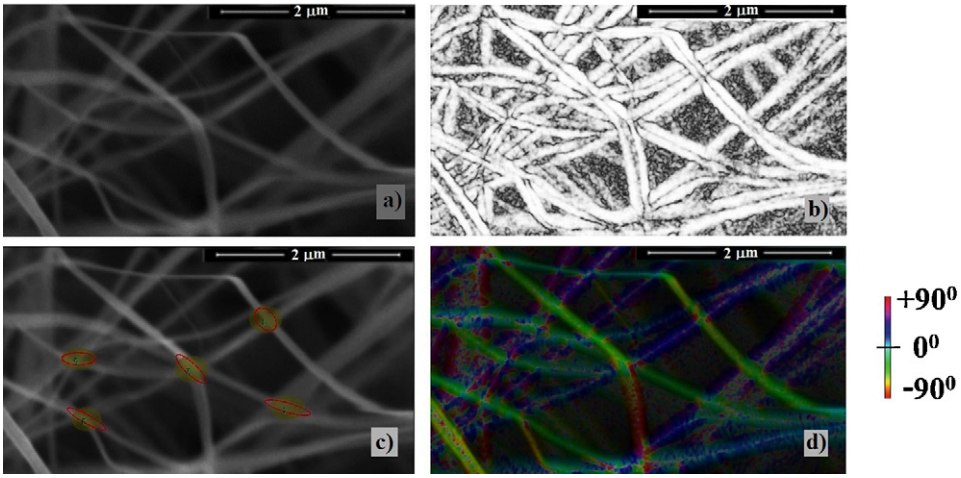


**Fig. 6.** (a) SEM micrograph (20,000×) of the fibers electrospun under optimized process parameters, (b) coherency map, (c) SEM micrograph (for calculation of coherency co-efficient and (d) HSB color-coded map. (For interpretation of the references to color in this figure legend, the reader is referred to the web version of the article.)

## 4. Conclusion

The present work vouched for the successful development of a BBD based response surface model for the prediction of diameter of electrospun cellulose acetate fibers. RSM and the applied experimental design could effectively determine the optimal values of the three chosen variables for theoretically obtaining electrospun CA fibers with minimal diameter. The chosen factors viz., potential difference, distance between tip and collector and feed rate exerted linear and quadratic influence on the fiber diameter. The successful location of optimum indicated the adequate choice of the experimental domain and the spacing of levels. The choice of a second order polynomial regression model was also satisfactory. The model can be used for devising strategies to fine tune the application-dependent shape-size accord of electrospun cellulose acetate fibers.

## Acknowledgements

The receipt of Canadian Commonwealth Scholarship from the Canadian Bureau for International Education (CBIE) and Department of Foreign Affairs and International Trade (DFAIT), Canada is thankfully acknowledged by Rocktotpal Konwarh. Gratitude is also extended to Department of Biotechnology (DBT), Government of India. The authors are also thankful to the Natural Sciences and Engineering Research Council (NSERC) Canada, Discovery Grant for the financial support to carry out this research. Mr. Jay Leitch is thankfully acknowledged for helping out in the SEM imaging.

## References

Amiraliyan, N., Nouri, M., & Kish, M. H. (2009). Electrospinning of silk nanofibers. I. An investigation of nanofiber morphology and process optimization using response surface methodology. *Fibers and Polymers*, *10*, 167–176.

Bezerra, M. A., Santelli, R. E., Oliveira, E. P., Villar, L. S., & Escaleira, L. A. (2008). Response surface methodology (RSM) as a tool for optimization in analytical chemistry. *Talanta*, *76*, 965–977.

Box, G. E. P., & Draper, N. R. (1987). *Empirical model building and response surfaces*. New York: John Wiley and Sons.

Chen, P.-C., Huang, X.-J., Huang, F., Ou, Y., Chen, M.-R., & Xu, Z.-K. (2011). Immobilization of lipase onto cellulose ultrafine fiber membrane for oil hydrolysis in high performance bioreactor. *Cellulose*, *18*, 1563–1571.

Chen, C., Wang, L., & Huang, Y. (2011). Electrospun phase change fibers based on polyethylene glycol/cellulose acetate blends. *Applied Energy*, *88*, 3133–3139.

Demir, M. M., Yilgor, I., Yilgor, E., & Erman, B. (2002). Electrospinning of polyurethane fibers. *Polymer*, *43*, 3303–3309.

Doshi, J., & Reneker, D. H. (1995). Electrospinnig process and applications of electrospun fibers. *Journal of Electrostatics*, *35*, 151–160.

Gu, S.-Y., & Ren, J. (2005). Process optimization and empirical modelling for electrospun poly(D,L-lactide) fibers using response surface methodology. *Macromolecular Materials and Engineering*, *290*, 1097–1105.

Haaland, P. D. (1989). Statistical problem solving. In P. D. Haaland (Ed.), *Experimental design in biotechnology* (pp. 1–18). New York: Marcel Dekker Inc.

Haas, D., Heinrich, S., & Greil, P. (2010). Solvent control of cellulose acetate nanofibre felt structure produced by electrospinning. *Journal of Materials Science*, *45*, 1299–1306.

Han, S. O., Youk, J. H., Min, K. D., Kang, Y. O., & Park, W. H. (2008). Electrospinning of cellulose acetate nanofibers using a mixed solvent of acetic acid/water: Effects of solvent composition on the fiber diameter. *Materials Letters*, *62*, 759–762.

Krishnappa, R. V. N., Desai, K., & Sung, C. M. (2003). Morphological study of electrospun polycarbonates as a function of the solvent and processing voltage. *Journal of Materials Science*, *38*, 2357–2365.

Lee, J. S., Choi, K. H., Ghim, H. D., Kim, S. S., Chun, D. H., Kim, H. Y., et al. (2004). Role of molecular weight of atactic poly(vinyl alcohol) (PVA) in the structure and properties of PVA nanofabric prepared by electrospinning. *Journal of Applied Polymer Science*, *93*, 1638–1646.

Megelski, S., Stephens, J. S., Chase, D. B., & Rabolt, J. F. (2002). Micro- and nanostructured surface morphology on electrospun polymer fibers. *Macromolecules*, *35*, 8456–8466.

Meyer, R. H., & Montogomery, D. C. (2002). *Response surface methodology: Process and product optimization using designed experiment* (2nd ed.). New York: John Wiley and Sons. (pp. 343–350).

Phachamud, T., & Phiriyawirut, M. (2011). In vitro cytotoxicity and degradability tests of gallic acid-loaded cellulose acetate electrospun fiber. *Research Journal of Pharmaceutical, Biological and Chemical Sciences*, *2*, 85–98.

Ramakrishna, S., Fujihara, K., Teo, W.-E., Lim, T.-C., & Ma, Z. (2005). *An introduction to electrospinning and nanofibers*. Singapore: World Scientific Publishing Co. Pvt. Ltd.

Ray, S., & Lalman, J. A. (2011). Using the Box–Behnken design (BBD) to minimize the diameter of electrospun titanium dioxide nanofibers. *Chemical Engineering Journal*, *169*, 116–125.

Rubenstein, D. A., Venkitachalam, S. M., Zamfir, D., Wang, F., Lu, H., Frame, M. D., et al. (2010). In vitro biocompatibility of sheath–core cellulose-acetate-based electrospun scaffolds towards endothelial cells and platelets. *Journal of Biomaterials Science*, *21*, 1713–1736.

Shin, E. H., Cho, K. S., Seo, M. H., & Kim, H. (2008). Determination of electrospun fiber diameter distributions using image analysis processing. *Macromolecular Research*, *16*, 314–319.

Shin, Y. M., Hohman, M. M., Brener, M. P., & Rutledge, G. C. (2001). Electrospinning: A whipping fluid jet generates submicron polymer fibers. *Applied Physics Letter*, *78*, 1149–1151.

Subbiah, T., Bhat, G. S., Tock, R. W., Parameswaran, S., & Ramkumar, S. S. (2005). Electrospinning of nanofibers. *Journal of Applied Polymer Science*, *96*, 557–569.

Vrieze, S. D., Camp, T. V., Nelvig, A., Hagström, B., Westbroek, P., & Clerck, K. D. (2009). The effect of temperature and humidity on electrospinning. *Journal of Materials Science*, *44*, 1357–1362.

Xiao, S., Wu, S., Shen, M., Rui, G., Huang, Q., Wang, S., et al. (2009). Polyelectrolyte multilayer-assisted immobilization of zero-valent iron nanoparticles onto polymer nanofibers for potential environmental applications. *ACS Applied Materials & Interfaces*, *1*, 2848–2855.

Zhao, S. L., Wu, X. H., Wang, L. G., & Huang, Y. (2004). Electrospinning of ethyl-cyanoethyl cellulose/tetrahydrofuran solutions. *Journal of Applied Polymer Science*, *91*, 242–246.